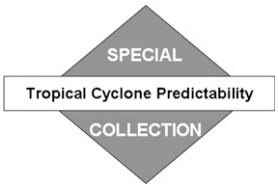

Sensitivity of Typhoon Forecasts to Different Subsets of Targeted Dropsonde Observations

FLORIAN HARNISCH AND MARTIN WEISSMANN

Deutsches Zentrum für Luft- und Raumfahrt, Institut für Physik der Atmosphäre, Oberpfaffenhofen, Germany

(Manuscript received 8 December 2009, in final form 3 February 2010)

ABSTRACT

For the first time, joint tropical cyclone (TC) surveillance missions by several aircraft were conducted in the western North Pacific basin within the framework of The Observing System Research and Predictability Experiment (THORPEX) Pacific Asian Regional Campaign (T-PARC) 2008. The collected dropsonde observations were divided into three different subsets depending on their location relative to the TC to investigate which observations are most beneficial for typhoon track forecasting. Data denial experiments with the European Centre for Medium-Range Weather Forecasts (ECMWF) global model were performed to analyze the influence of the different dropsonde subsets. In these experiments, the largest TC track forecast improvements are found for observations in the vicinity of the storm, placed at a circular ring at the outer boundary of the TC. In contrast, observations in remote regions indicated to be sensitive by singular vectors seem to have a relatively small influence with a slight positive tendency on average. Observations in the TC core and center lead to large analysis differences, but only very small mean forecast improvements. This is likely related to the fact that even modern high-resolution global models cannot fully resolve the TC center and thus can only use a relatively small part of the information provided by observations within the TC center. Times prior to landfall and recurvature are stronger affected by additional observations, while the influence on the track forecast after recurvature is relatively weak.

1. Introduction

Tropical cyclones (TCs) usually develop over data-sparse regions of the tropical oceans. The limited number of observations and the rapid development of TCs increases uncertainties of the model analysis in these regions, which can lead to significant forecast errors (Langland 2005).

Surveillance programs deploying dropsonde observations in and around TCs have been operated for the Atlantic (Burpee et al. 1996; Aberson 2002) and the western North Pacific basin (Wu et al. 2005). Several studies showed that despite the increased use of satellite data in the analysis of numerical weather prediction models, additional dropsonde measurements of key variables such as wind, temperature, and humidity in the environment of TCs can lead to improvements of TC track forecasts of the order of 10%–20% (Aberson 2003; Wu et al. 2007b; Yamaguchi et al. 2009). Despite the average reduction of track forecast errors, single cases occur where additional observations do not reduce the errors due to the stochastic nature of data assimilation and the use of observations close to a TC, which cannot be correctly represented by the resolution of current global models (Wu et al. 2007b; Aberson 2008).

To deploy extra observations in the most beneficial way, adaptive observing guidance based on the findings of different targeting techniques as singular vector (SV) calculations (Buizza and Montani 1999; Peng and Reynolds 2006; Reynolds et al. 2009), ensemble transform Kalman filter (ETKF) products (Majumdar et al. 2006), and adjoint calculations (Wu et al. 2007a) have been used over the last few years. A detailed comparison of the different targeting techniques for the western North Pacific basin is given in Wu et al. (2009) and for the Atlantic in Majumdar et al. (2006) and Reynolds et al. (2007).

Corresponding author address: Florian Harnisch, Deutsches Zentrum für Luft- und Raumfahrt, Institut für Physik der Atmosphäre, Oberpfaffenhofen, 82234 Wessling, Germany.
E-mail: florian.harnisch@dlr.de

DOI: 10.1175/2010MWR3309.1

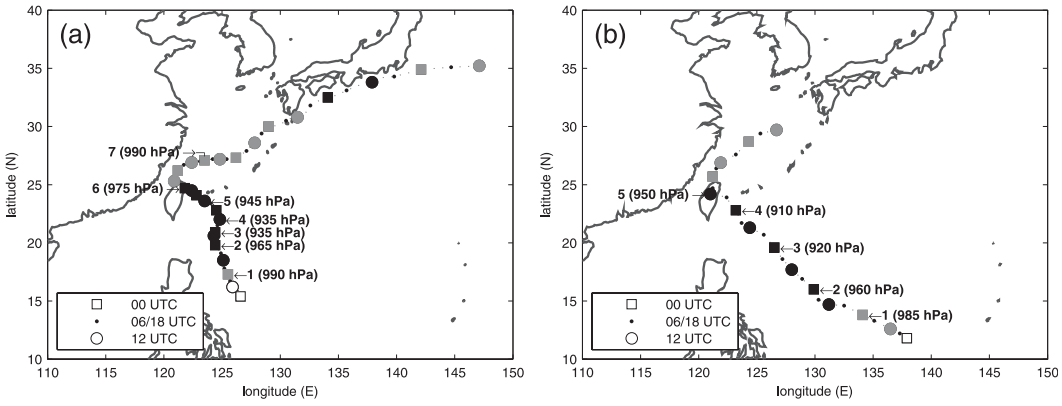

FIG. 1. JMA best-track data of (a) Typhoon Sinlaku from its genesis on 8 Sep 2008 until its extratropical transition on 20 Sep 2008 and (b) Typhoon Jangmi from 24 Sep 2008 to 30 Sep 2008. Rectangles indicate the position of the typhoon at 0000 UTC, circles at 1200 UTC, and dots at 0600 and 1800 UTC, respectively. The shading of the markers indicates the classification of the TC: (black) typhoon intensity and (gray) tropical or severe tropical storm. Times with data denial experiments are emphasized by the corresponding case number (see also Table 1) and the central mean sea level pressure.

The multinational The Observing System Research and Predictability Experiment (THORPEX) Pacific Asian Regional Campaign (T-PARC; Parsons et al. 2008) in cooperation with the Tropical Cyclone Structure (TCS08) field experiment (Elsberry and Harr 2008) took place in the western North Pacific basin from August to October 2008. A strong effort was given to combine research activities for extensive measurements of TCs. The aims were to increase the understanding of TC formation, intensification, structure change, and extratropical transition, as well as to improve the forecast skill of TCs. An unprecedented set of observational platforms of different research aircraft [e.g., the U.S. Air Force WC-130, the Naval Research Laboratory (NRL) P-3, and the Deutsches Zentrum für Luft- und Raumfahrt (DLR) Falcon 20] in combination with driftsonde gondolas, research vessels, and extra satellite observations was operated. Systematic observations targeted around tropical cyclones during the full life cycle of a storm from the genesis in tropical waters throughout the northwestward movement, recurvature, and extratropical transition were conducted. In collaboration with T-PARC, the Taiwanese Astra Jet was operated under the research program Dropwindsonde Observations for Typhoon Surveillance near the Taiwan Region (DOTSTAR), where dropsonde observations are deployed operationally on TCs that pose a threat to the Taiwanese island (Wu et al. 2005, 2007b).

This study investigates the benefit of T-PARC dropsonde observations in different locations on the basis of data denial experiments with the European Centre for Medium-Range Weather Forecasts (ECMWF) Integrated Forecasting System (IFS). In these experiments, the division of dropsondes into different subsets should yield information about the importance of observations in certain areas relative to the position of the TC.

Two major typhoon systems during the T-PARC period are investigated in this study: Typhoon Sinlaku and Typhoon Jangmi (Fig. 1). Sinlaku developed around 8 September 2008 east of the Philippines. The storm moved slowly northward to the west of the subtropical

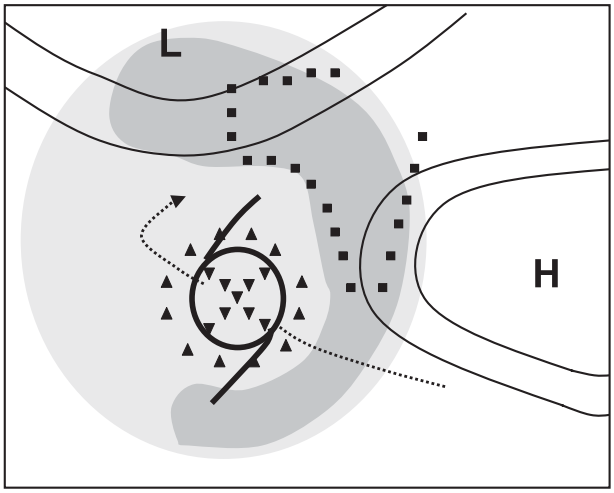

FIG. 2. Idealized sketch illustrating the separation of the dropsondes into different subsets. Dropsonde positions are labeled by downward-pointing triangles (core and center of the TC), squares (remote sensitive region), and upward-pointing triangles (vicinity of the TC). Shading indicates the typical pattern of regions with high (dark gray) and moderate (light gray) sensitivity during T-PARC period calculated by singular vectors. Solid lines mark possible streamlines, representing the midlatitude flow north of the tropical cyclone and the subtropical anticyclone to the east. The trajectory of the TC is shown as a dotted line.

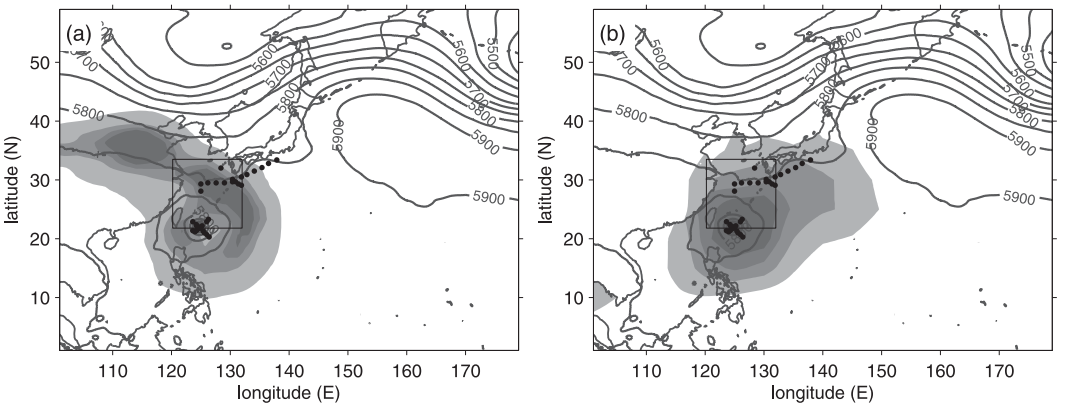

FIG. 3. Targeting guidance for Typhoon Sinlaku valid at 1200 UTC 11 Sep 2008 initialized at 0000 UTC 9 Sep 2008 with 36-h optimization time. The areas of 1, 2, 4, and 8×10^6 km^2 are shaded. (a) SV-based calculation of the ECMWF model and (b) ETKF multimodel (NCEP/ECMWF/CMC) ensemble output. The verification region (black box) is centered around the expected position of the TC. Black contour lines show the geopotential height at 500 hPa and black dots, the location of dropsondes.

anticyclone and hit Taiwan on 14 September. After recurving between Taiwan and China, Sinlaku first struggled to speed up, but then moved on toward Japan with the subtropical anticyclone to the southeast. The storm reintensified again before passing south of Japan and then transitioned to an extratropical system. Seven cases during the period 9–16 September were chosen for data denial experiments (Fig. 1a). Typhoon Jangmi developed between Guam and the Philippines around 23 September, then moved to the northwest and struck Taiwan on 28 September. Jangmi experienced a strong weakening during landfall, recurved close to the Chinese coast, and afterward dissolved south of Japan. Five times were selected for data denial experiments during the period 25–28 September (Fig. 1b).

Section 2 gives a description of the ECMWF global model, the setup of the data denial experiments, and the definition of the TC position calculation. Results of the track and intensity forecasts of Sinlaku and Jangmi and statistics of the assimilation of dropsondes released in the center and core of Typhoon Sinlaku are shown in section 3. The discussion and summary is presented in section 4.

2. Method

a. Model system

The data denial experiments were performed using the spring 2009 version of the ECMWF IFS (cycle 35r2). The horizontal resolution of the experiments was T_L799 (~25 km) and 91 vertical levels were used. A detailed description of the ECMWF four-dimensional variational data assimilation scheme can be found in Rabier et al. (2000), Mahfouf and Rabier (2000), and Klinker et al. (2000). The 12-hourly assimilation windows between 2100–0900 and 0900–2100 UTC were used for the nominal assimilation times at 0000 and 1200 UTC, respectively. The dropsonde quality control consists of a first-guess check performed prior to the main analysis to reject likely wrong observations (Järvinen and Undèn 1997), where observations are rejected if their expected variance of the normalized first-guess departures exceeds predefined limits. Weakened constraints for the first-guess check, which are operationally applied to a region up to 30°N to avoid very high rejection rates within and near TCs, were extended up to 40°N because of the reintensification of Sinlaku near of 30°N. In practice, the first-guess check for dropsondes was inactive in this region. During the assimilation, a variational quality control (VarQC) procedure (Andersson and Järvinen 1999) is applied, where the cost function is modified by reducing the weight of the observations with large first-guess departures. The VarQC procedure does not irrevocably reject observations and the weight of the observations can be increased again during later iterations.

b. Experimental design

Observations of wind, temperature, and specific humidity from dropsondes were fed into the ECMWF data assimilation system after correcting dropsonde timing errors that occurred in the operational ECMWF assimilation. A control run (''NoObs'') without any dropsonde observations was performed for the whole period of Typhoon Sinlaku and Typhoon Jangmi. Additionally, experiments initialized from the control run that use certain parts of the observations or all observations were conducted for selected cases. These cases were chosen under the conditions of a strong typhoon and a large

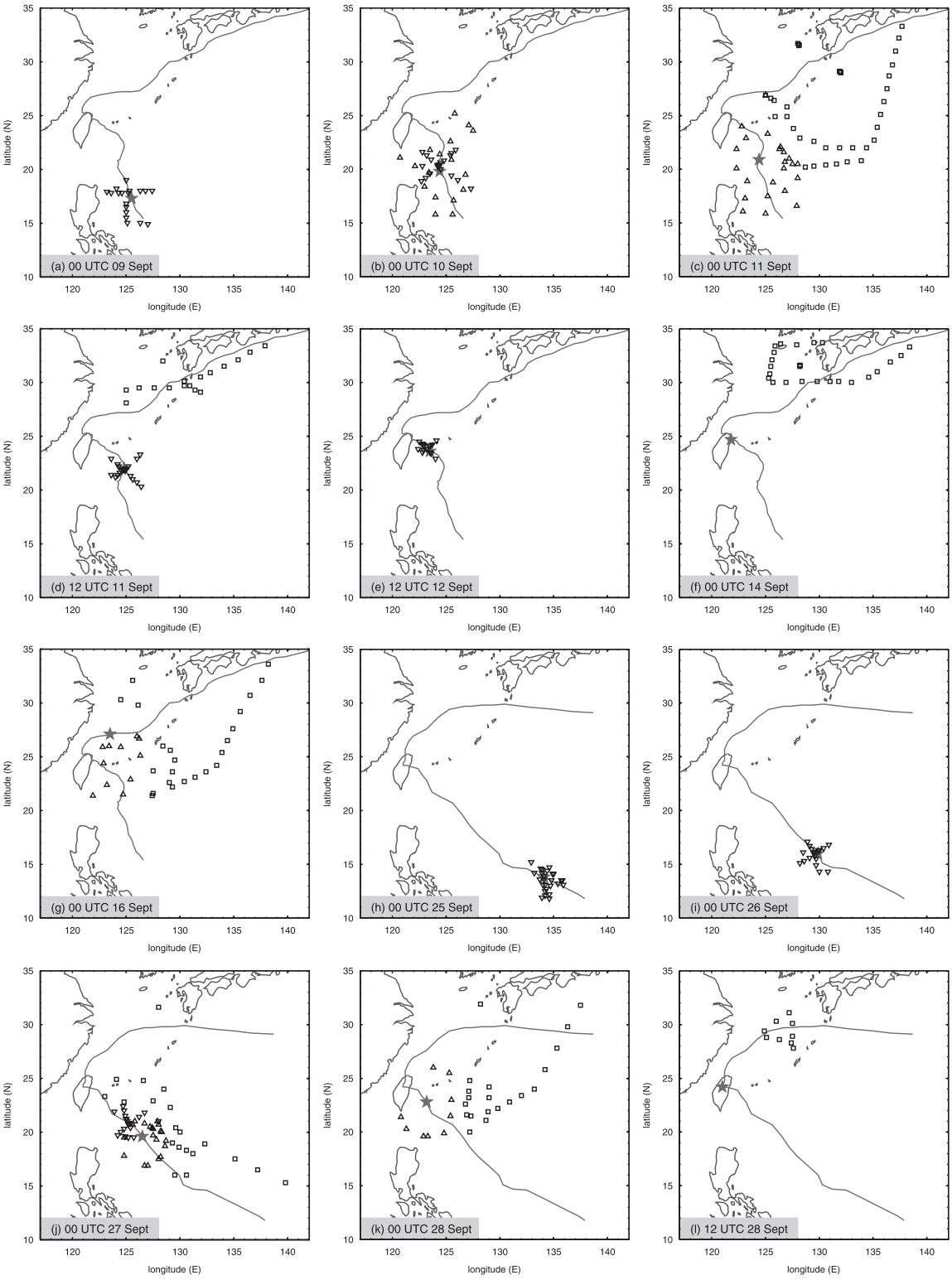

FIG. 4. Position of dropsondes used in the data denial experiments for (a)–(g) Typhoon Sinlaku and (h)–(l) Typhoon Jangmi (see also Table 1): best track of the respective typhoons (solid gray line) and the actual position of the storm (gray stars). Note that the storm position at nominal time is displayed, while the dropsondes can be distributed within the 12-hourly assimilation window. Squares, upward-pointing triangles, and downward-pointing triangles represent dropsondes of ReObs, ViObs, and CeObs, respectively.

TABLE 1. Overview of number of dropsondes in different experiments. Forecast times denote the interval in which the track forecasts of the Typhoons Sinlaku and Jangmi (2008) were evaluated. Case numbers refer to the best tracks shown in Fig. 1.

Case No.	Initial time–date	Forecast times (h)	ReObs	ViObs	CeObs	allObs
1	0000 UTC 9 Sep	12–120			18	
2	0000 UTC 10 Sep	12–120		17	20	37
3	0000 UTC 11 Sep	12–120	37	22		59
4	1200 UTC 11 Sep	12–120	17		19	36
5	1200 UTC 12 Sep	12–120			22	
6	0000 UTC 14 Sep	12–120	25			
7	0000 UTC 16 Sep	12–108	23	11		34
8	0000 UTC 25 Sep	12–120			26	
9	0000 UTC 26 Sep	12–84			19	
10	0000 UTC 27 Sep	12–84	20	20	20	60
11	0000 UTC 28 Sep	12–60	20	9		29
12	1200 UTC 28 Sep	12–48	9			

number of dropsonde data in the area of the storm. Data denial experiments were performed to investigate the sensitivity of the model analysis and forecast to observations taken in three distinct areas relative to the TC position. Figure 2 presents a schematic picture of the partitioning of the observations. The shading indicates a sensitivity pattern often highlighted by SV calculations during T-PARC with sensitivity maxima 700–1200 km away from the TC center. The DLR Falcon mainly sampled these sensitive regions. The observations in the core and center primarily consist of WC-130 dropsondes, while the observations in the vicinity of the typhoon were primarily taken by the DOTSTAR aircraft. In addition, the DOTSTAR aircraft also covered parts of the sensitive regions on several days. The different subsets of observations also contain a small number of NRL P-3 dropsondes in some cases. Note here that the DOTSTAR aircraft and the DLR Falcon were flying in the upper troposphere, while the NRL P-3 and the WC-130 were mainly flying in the lower troposphere for the dropsonde deployment on the days discussed in this study. Experiments with observations in remote sensitive regions are called ''ReObs'' experiments, those with observations in the vicinity of the typhoon are called ''ViObs'' experiments, and those with observations in the center and core region are called ''CeObs'' experiments.

In practice, this clear separation of observations is not always as unambiguous as shown in Fig. 2 and is partly based on a subjective assessment. An argument for the separation of the observations evolves from the targeting guidance. Several targeting guidance products, ranging from SV calculations of different models over ETKF products to adjoint calculations, were available during T-PARC. An example of two targeting guidance products valid at 1200 UTC 11 September is shown in Fig. 3. Sinlaku is located southeast of Taiwan (see also Fig. 1) and the predicted position of landfall on Taiwan and recurvature is uncertain. Similar sensitivity patterns are frequently identified before recurvature of Typhoons Sinlaku and Jangmi. The SV calculations indicate maximum sensitivity to the north and northeast of Sinlaku linked to the interface of the storm with the midlatitude flow and the edge of the subtropical ridge to the east. A

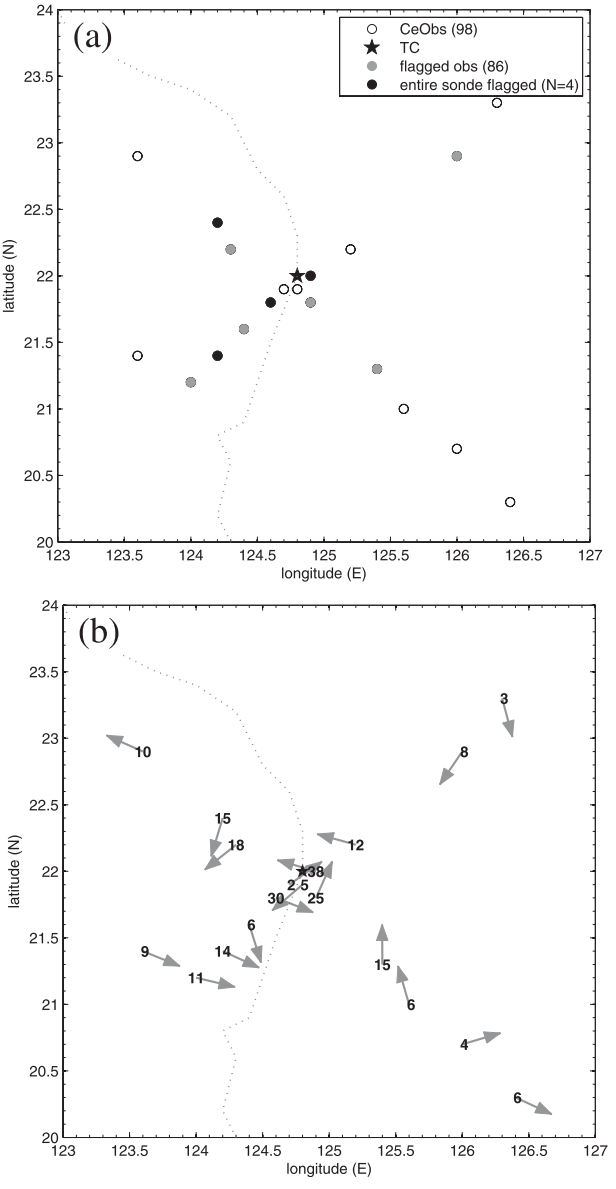

FIG. 5. Wind observations of dropsondes used for the CeObs subset at 1200 UTC 11 Sep 2008. (a) Position of the dropsondes: white shading indicates that all wind observations of the sounding are used, light gray shading that they are partially used, and dark gray that all wind observations from the sounding are flagged by VarQC. (b) First-guess departures (difference of observed value and first-guess field) averaged over every dropsonde between 650 and 1000 hPa for wind speed in m s^{-1} and wind direction (gray arrows).

TABLE 2. Number of dropsonde wind, temperature, and specific humidity observations included in the CeObs experiment at 1200 UTC 11 Sep 2008.

			Data flagged by	
	All data	No flag	First-guess check	VarQC
Wind speed	184	98	0	86
Temperature	113	98	0	15
Specific humidity	123	122	0	1

second maximum upstream indicates sensitivity to the approaching trough structure over northern China. The sensitivity is lower close to the TC and a relative minimum is visible next to the TC center. In contrast, the ETKF computation shows a sensitivity maximum at the center of the TC. The sensitivity decreases with distance to the storm and is elongated from the southwest to the northeast. At that targeting time, two aircraft were flying and dropsondes were released north of the TC (ReObs) and close to the center and core of the TC (CeObs).

Figure 4 and Table 1 show the available dropsonde data for all selected cases. The number of soundings used for the individual experiments varies from 9 to 37. When observations were separated into two or three subsets, an additional experiment using all observations (''allObs'') was performed.

c. *Definition of the TC position*

The TC position is computed by searching for the subgrid minimum of mean sea level pressure (MSLP) in the western North Pacific domain. The definition of the TC position as minimum MSLP shows no significant differences compared to the result of the operational ECMWF TC tracker algorithm (Van der Grijn et al. 2005). In general, the TC position definition by MSLP is reliable over the ocean, but can lead to errors when the TC reaches the complex orography of Taiwan with mountains up to 4000 m. Typhoon Jangmi is located directly over Taiwan at 1200 UTC 28 September (Fig. 1b). A secondary low in the model forecast affects the position calculation of the TC from the MSLP fields. Thus, the minimum of the geopotential height at 700 hPa instead of the MSLP is used to define the TC position in order to minimize the interference with the topography of Taiwan. This is confirmed by the visual interpretation of analysis fields.

3. Results

a. *Assimilation statistics of TC center and core observations*

The U.S. Air Force WC-130 conducted several flights penetrating Sinlaku and Jangmi and released dropsondes in the core and eyewall region. Data denial experiments

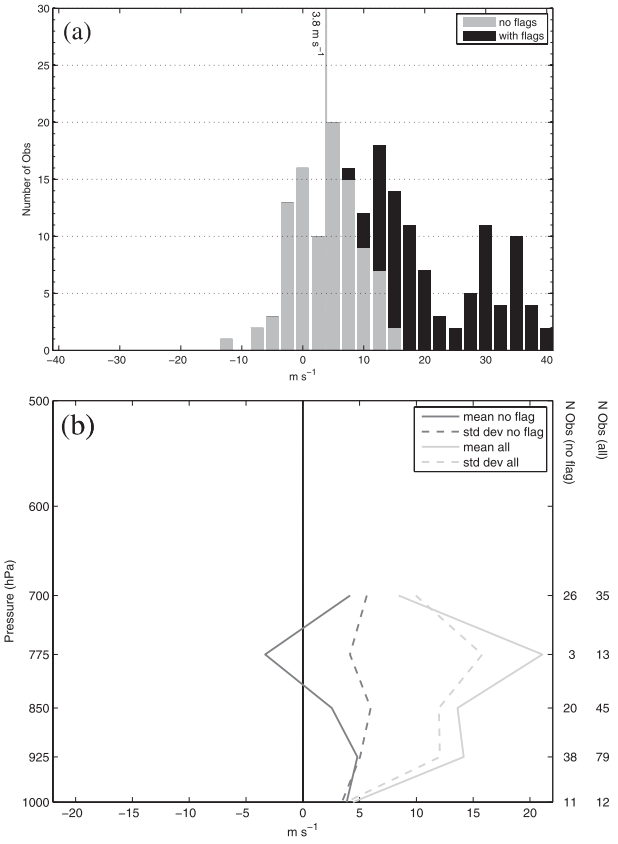

FIG. 6. First-guess departures of observed wind speeds for soundings displayed in Fig. 5 at 1200 UTC 11 Sep 2008. (a) Histogram of wind speed first-guess departures. The vertical line illustrates the mean value of used data. (b) Vertical profile of standard deviation and mean of all and used (no flag) first-guess departures.

only using these observations (CeObs) were performed 4 times during Typhoon Sinlaku and 3 times during Typhoon Jangmi (Table 1) to investigate the benefit of such observations.

CeObs dropsondes were often released on two straight flight legs crossing the typhoon. In the example shown in Fig. 5a, nearly 50% of the wind observations are detected and flagged by VarQC, which reduces the weight of observations in the analysis. In practice, the flagged observations have very low weights and are basically not used. As mentioned in section 2a the first-guess check is relaxed for TC sondes and effectively inactive (Table 2). Similar rejection rates are also seen for other analysis times with CeObs observations.

The average wind speed first-guess departure of each single sounding (difference between the wind speed observations from one sounding and the first-guess field) is plotted in Fig. 5b. All dropsondes show significantly higher wind speeds compared to the first-guess field and enhance the developed cyclonic wind structure around the TC. The histogram of the wind speed first-guess

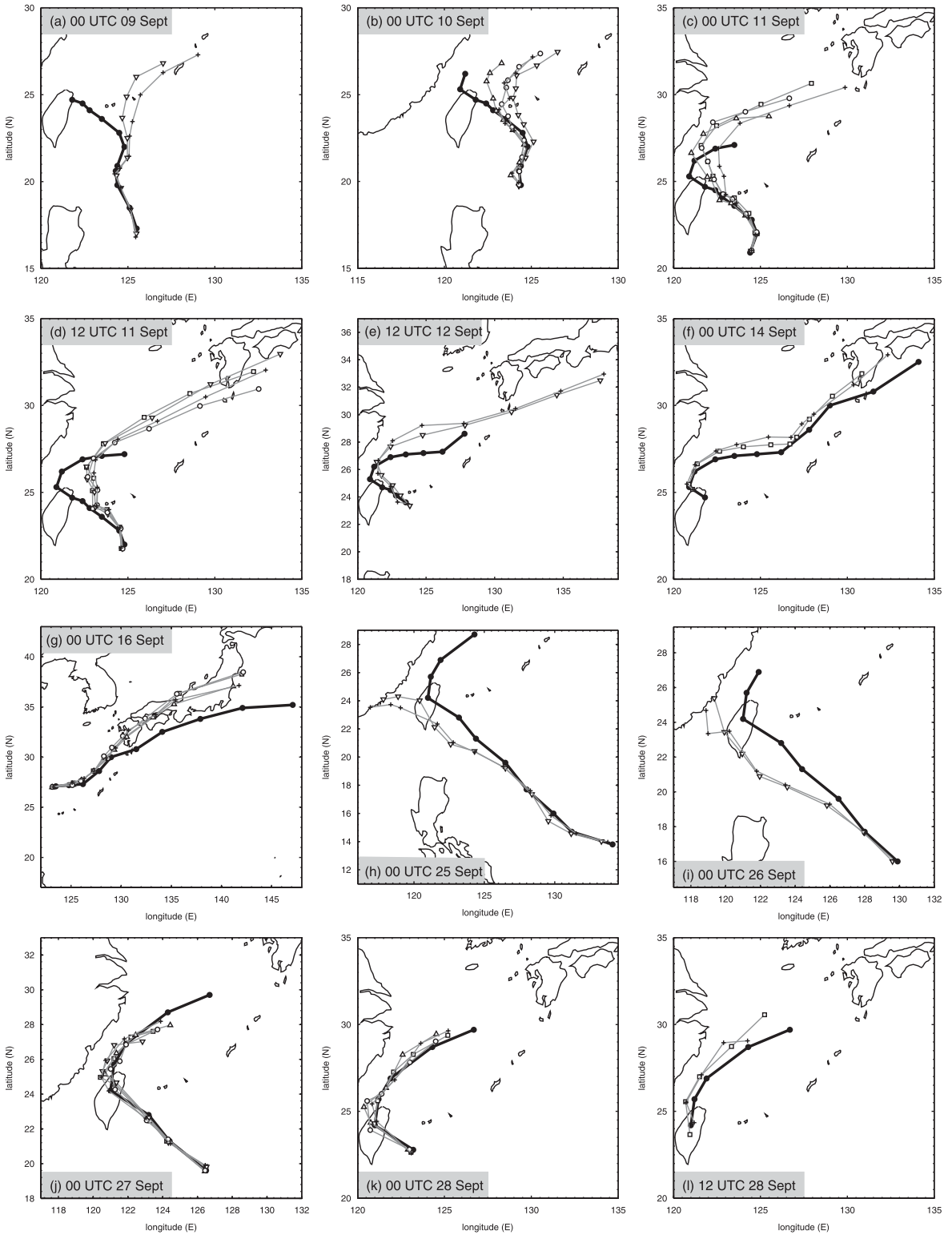

FIG. 7. Track forecasts of all experiments for (a)–(g) Typhoon Sinlaku and (h)–(l) Typhoon Jangmi (see also Table 1). TC positions are plotted every 12 h. Black solid dots display the best-track data. Squares, upward-pointing triangles, downward-pointing triangles, and circles represent forecasts of ReObs, ViObs, CeObs, and allObs, respectively. Cross markers show the forecast of the NoObs control experiment. Corresponding track forecast errors can be found in Tables 3 and 4.

departures (Fig. 6a) shows a high number of first-guess departures exceeding 10 m s^{-1}. Most of these large first-guess departures are high wind speeds in the eyewall region. First-guess departures greater than 15 m s^{-1} appear too extreme for the data assimilation and are rejected by VarQC. The distribution of accepted wind speed first-guess departures still has a positive mean value of 3.8 m s^{-1}, but is of more Gaussian shape as the positive extremes are rejected by the VarQC.

The vertical distribution of the wind speed first-guess departures is shown in Fig. 6b. During the crossing of the TC center, the WC-130 was flying at low levels. Thus, sounding data are only available below 700 hPa. First-guess departures larger than 10 m s^{-1} can be identified above the surface layer. After the VarQC procedure, the first-guess departures are reduced to less than 5 m s^{-1}, but the used observations still lead to an intensification of the cyclonic wind speeds at most levels.

In contrast to wind speed, humidity and temperature observations show much lower first-guess departures (not shown) and a larger percentage of the data are used (Table 2).

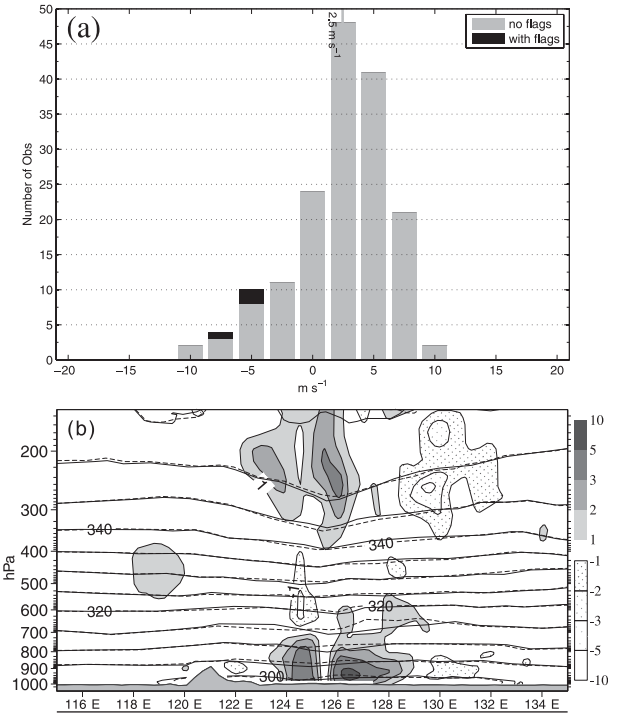

FIG. 8. (a) Histogram of wind speed first-guess departures for soundings displayed in Fig. 4a at 0000 UTC 9 Sep 2008. (b) Cross section of the analysis valid at 0900 UTC 10 Sep 2008. The cross section is located at 16.9°N, which is approximately the center of the TC in the experiments and ranges from 115° to 135°E. The wind speed difference (m s^{-1}) of the CeObs and the NoObs experiment (shaded) are plotted with positive values indicating higher wind speeds in the CeObs experiment. Solid (dashed) lines show the analysis of the isentropes (K) of the CeObs (NoObs) experiment. Gray shading at the bottom represents the topography.

b. Typhoon track forecasts

1) PRERECURVATURE PERIOD

During the prerecurvature stage of Sinlaku (9–14 September), high forecast uncertainty is linked to the location of landfall and recurvature and to the predicted movement of the system after recurvature. This period also shows the largest influence of dropsondes on the track forecast (Fig. 7, Tables 3 and 4). In the following, individual cases, representative for the other times, are discussed.

The first case of Sinlaku (0000 UTC 9 September, Fig. 7a) is at the time of the beginning intensification. The CeObs experiment produces an improvement of the forecasted storm track and a 12–120-h mean track forecast error reduction of 24% is achieved. The storm is classified as a tropical storm with a central pressure of 990 hPa (Fig. 1a), which causes moderate first-guess departures of wind speed (<10 m s^{-1}) and only three observations are flagged and rejected (Fig. 8a). Figure 8b shows that the CeObs experiment increases the low-level wind speed around Sinlaku (located at ~125.5°E). Even though the dropsondes of the CeObs experiment are located in the lower troposphere, the CeObs analysis increments extend into the upper troposphere and modify the wind and the temperature fields (Fig. 8b).

At 0000 UTC 10 September (Fig. 7b), observations located in the vicinity of the storm (ViObs) lead to a much better track forecast compared to the control run. With these observations, the storm forecast is shifted farther to the west, which is closer to the best track. A 12–120-h mean track forecast error reduction of 36% is obtained. In contrast, the track forecast of the CeObs experiment shows an eastward shift of the typhoon track. The track of the CeObs experiment is worse than the one of the control run and leads to an average 12–120-h track forecast error increase of 51%. The allObs run is still dominated by the negative effect of the CeObs observations and results in a mean 12–120-h track forecast degradation of 17%.

The analysis of the CeObs run shows a stronger developed typhoon with higher wind speeds at 850 hPa on the southwestern side of the storm compared to the control run (Figs. 9a,d). While this region of increased wind speed can be identified also in the allObs run (Fig. 9c), it is not apparent at the ViObs run (Fig. 9b). The increased cyclonic low-level winds in the southwestern sector of the TC apparently do not have a positive effect on the track forecast. The deep-layer environmental flow seems to be of higher importance for the steering of the typhoon.

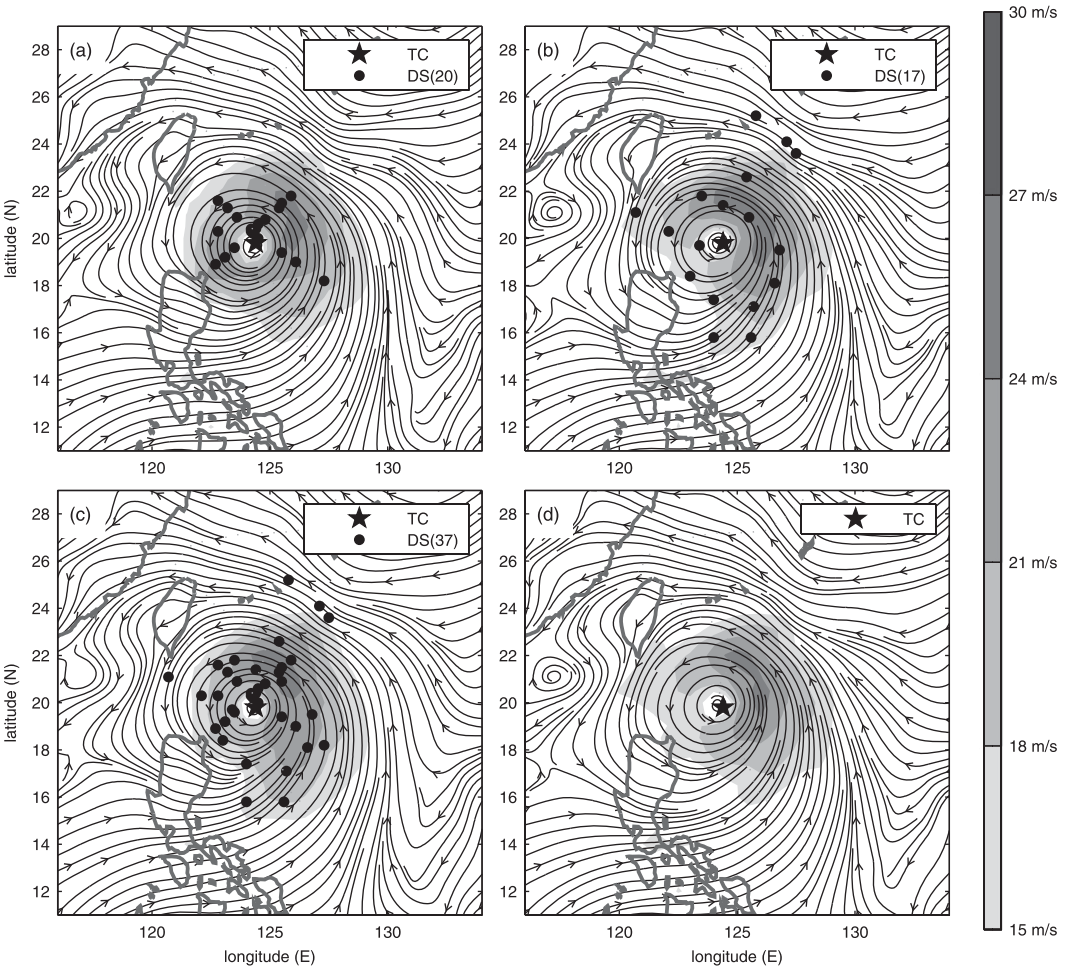

FIG. 9. Analysis of streamlines and wind speed (shading) at 850 hPa at 0000 UTC 10 Sep 2008 for (a) the CeObs experiment, (b) the ViObs experiment, (c) the allObs experiment, and (d) the control experiment. Best-track position of the TC is indicated by a black star and the location of the dropsondes by black dots.

Figure 10 illustrates the analysis of the geopotential height at 500 hPa for the experiments and the control run as well as the deep-layer (850–300 hPa) mean wind difference between the experiments and the control run. The CeObs experiment (Fig. 10a) shows a less distinct edge of the subtropical high east of Sinlaku and a larger eastward flow component southeast of the storm than the control run. In the ViObs experiment (Fig. 10b), the flow southeast of the storm contains a larger westward component, which seems to shift the track farther to the west and produces a better track forecast. A more northward wind component to the southeast of Sinlaku can be identified in the allObs run (Fig. 10c). The ECMWF SV calculation also shows a band of maximum sensitivity south and east of Sinlaku (Fig. 11a), which confirms the sensitivity of the steering flow in the region south and east of Sinlaku. The 72-h forecasts of the geopotential height at 500 hPa and the deep-layer mean wind is displayed in Fig. 12. The time step corresponds to the time when the track forecasts of the different experiments start to diverge (cf. Fig. 7b). The forecast shows differences of the edge of the subtropical high to the east of Sinlaku as well as of the position of the storm. The subtropical high is developed weakest in the CeObs experiment (Fig. 12a), which allows Sinlaku to move to the northeast. The highest wind speeds of the deep-layer mean wind are found east and northeast of Sinlaku in the CeObs experiment supporting the northeastward movement. Comparing the allObs and ViObs experiments (Figs. 12b,c), one can identify differences in the structure of the storm and slightly higher wind speeds in the ViObs experiment west of Sinlaku, which seem to be responsible for the smaller track forecast errors in the ViObs experiment.

Observations in the vicinity of the typhoon again led to an improved track forecast of Sinlaku initialized at

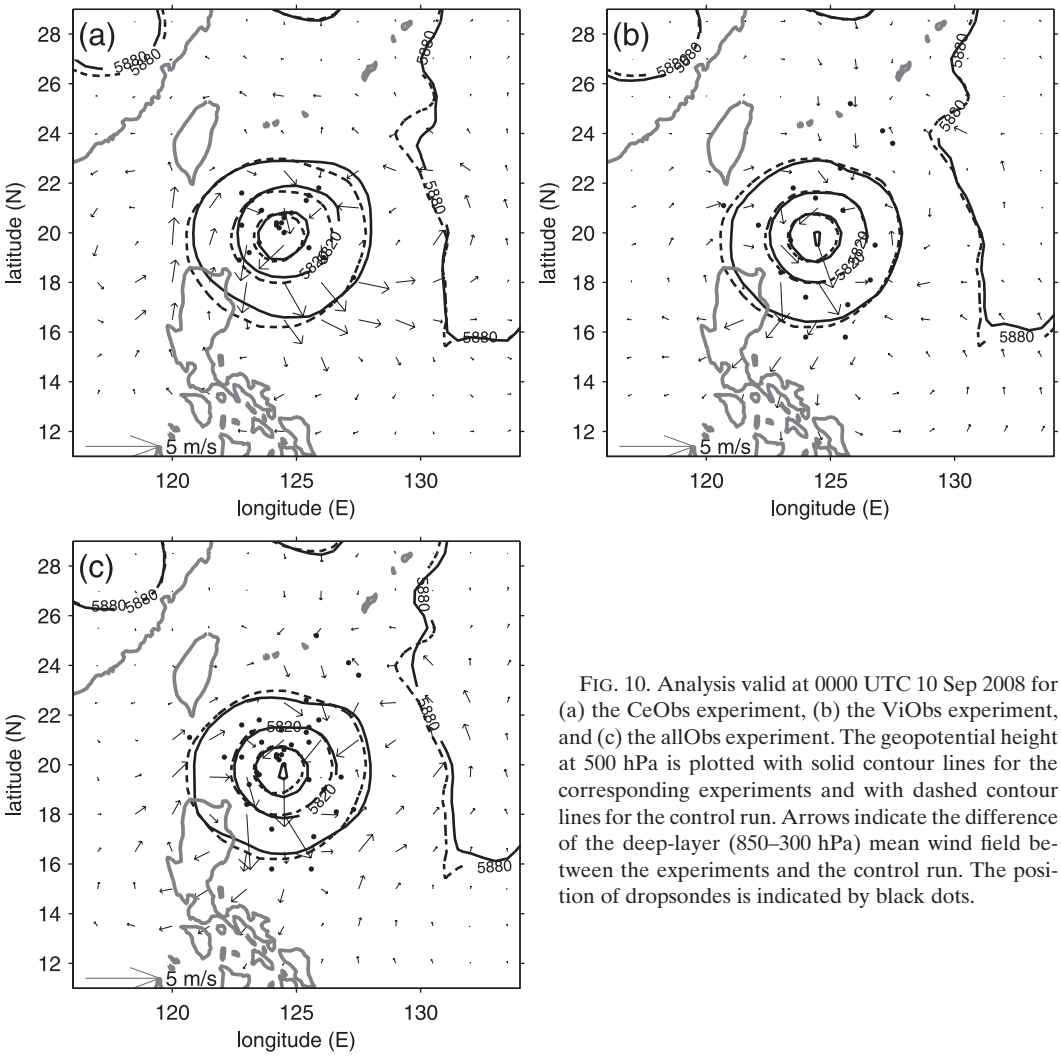

FIG. 10. Analysis valid at 0000 UTC 10 Sep 2008 for (a) the CeObs experiment, (b) the ViObs experiment, and (c) the allObs experiment. The geopotential height at 500 hPa is plotted with solid contour lines for the corresponding experiments and with dashed contour lines for the control run. Arrows indicate the difference of the deep-layer (850–300 hPa) mean wind field between the experiments and the control run. The position of dropsondes is indicated by black dots.

0000 UTC 11 September (Fig. 7c). The track forecast of the control run is already very accurate up to 48 h, but the track forecast from 2 days onward is improved with the ViObs observations. The landfall scenario of Sinlaku at the northern tip of Taiwan is predicted correctly and also the representation of the motion during recurvature is more similar to the best-track scenario. ReObs observations at the same time shift the track closer to the best track, but keep the storm a little farther to the east during recurvature (Fig. 7c). Again, the combination of the two subsets does not show the best performance and the 12–120-h mean track forecast error reduction of allObs is 28%, while 16% can be achieved with the ReObs run and 51% with the ViObs run. Despite the improvement of the track until the recurvature of the storm, the model seems to have problems with the propagation of Sinlaku after recurvature. From 84 h onward, a timing error of all track forecasts is observed (Fig. 7c). Even if the track forecast error is reduced with extra observations, the error due to the acceleration of the storm is large and dominates.

Experiments for the prerecurvature period of Typhoon Jangmi do not show such a positive influence as for Sinlaku. The southwestward bias of the track forecast is hardly corrected in the CeObs experiment during the early stages (Figs. 7h,i). However, no ViObs observations are available for these two cases. Results at 0000 UTC 27 September indicate that the track forecast of the control experiment is very accurate and landfall is predicted at the correct position. After landfall, all the experiments struggle to accelerate Jangmi. These propagation errors of Sinlaku and Jangmi after landfall and recurvature are likely linked to model deficiencies of the land interaction of the typhoon and the connected structure change on its way over land rather than errors in the initial conditions. However, a better representation of the TC in the initial

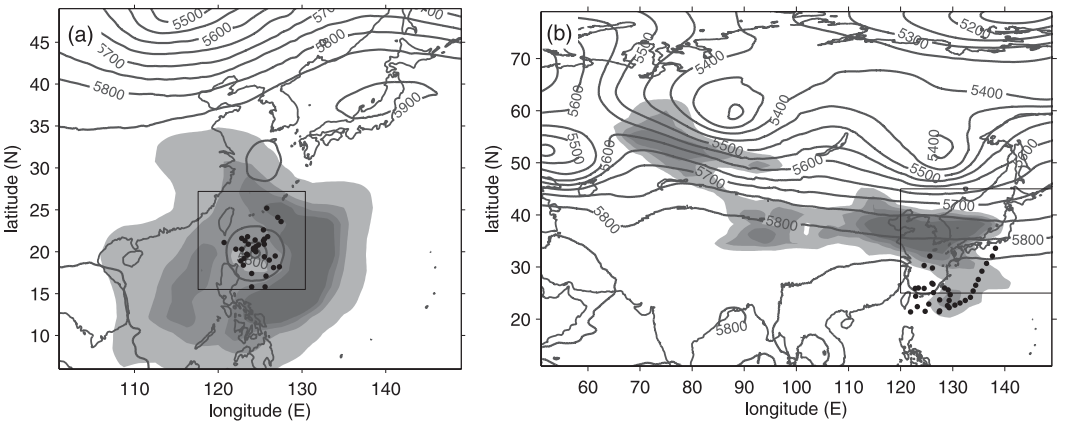

FIG. 11. Targeting guidance based on SV calculation of the ECMWF model for Typhoon Sinlaku valid at (a) 0000 UTC 10 Sep 2008 initialized at 0000 UTC 8 Sep 2008 with 48-h optimization time and (b) 0000 UTC 16 Sep 2008 initialized at 0000 UTC 14 Sep 2008 with 72-h optimization time. The areas of 1, 2, 4, and 8×10^6 km^2 are shaded. The verification region is shown by a black box. Black contour lines show the geopotential height at 500 hPa and black dots the location of dropsondes.

conditions due to extra observations can also lead to a more correct structure and track change during the land passage (Wu 2001). When the landfall point is represented best in the model, the errors due to land interaction can also be minimized resulting in smaller timing errors, as in the ViObs experiment initialized at 1200 UTC 11 September.

2) POSTRECURVATURE PERIOD

The influence of the observations after recurvature is generally smaller than before recurvature. In several cases (Figs. 7f,g,l), the control run already shows a very accurate track forecast. Slight modifications of the track forecast can be achieved with different subsets of observations, but no striking feature can be identified. During this stage of the TC propagation, the flow field upstream in the midlatitudes becomes more important for the track forecast and the influence of dropsondes in the TC environment seems to weaken.

Errors in the predicted upstream flow field appear to dominate the cases in the postrecurvature period of Sinlaku. The track forecast of the ViObs, ReObs, allObs, and the control experiment at 0000 UTC 16 September is very accurate up to 48 h (Fig. 7g) with track errors less than 70 km (Table 3). After 48 h, the track errors of all experiments increase significantly, but there is only a little difference between the experiments. Figure 13 shows that none of the experiments predicts the shortwave trough and the flow structure over northern China at 48 h correctly. The differences between the forecasts of the experiments and the control run seem negligible compared to the differences between the forecasts and the verifying analysis. The forecast error related to the trough structure evolves from a region far upstream over western Siberia, which is also indicated to be sensitive by ECMWF SV calculations (Fig. 11b). This error is not affected by changes in the initial conditions close to the storm, which explains the low influence of dropsondes next to Sinlaku in this case.

The propagation error of Sinlaku after recurvature in the forecast initialized at 1200 UTC 11 September is to some extent also related to errors in the upstream midlatitude flow (not shown).

3) OVERALL INFLUENCE

Scatter diagrams summarizing the results for all individual cases are displayed in Fig. 14. The ViObs subset leads to the highest reduction of the track forecast errors. Large values of track error reduction could be achieved in most cases, and the linear fit as well as the averaged values indicates a positive influence especially from 2 days onward. In the CeObs experiments, the points are distributed around the 45° line. Average values as well as the linear fit show a slight positive influence of these observations overall, but large positive and negative outliers are apparent. For the ReObs experiments, the overall influence is rather neutral with a slight positive tendency, comparable to the CeObs results. Combining the subsets together does not automatically improve the track forecast more than when using only one subset. The allObs experiment also results in a positive influence on average, but not as large as the ViObs experiment.

c. Typhoon intensity forecast

The correct intensity forecast of the TC is of high importance. Large errors in the models are expected, as

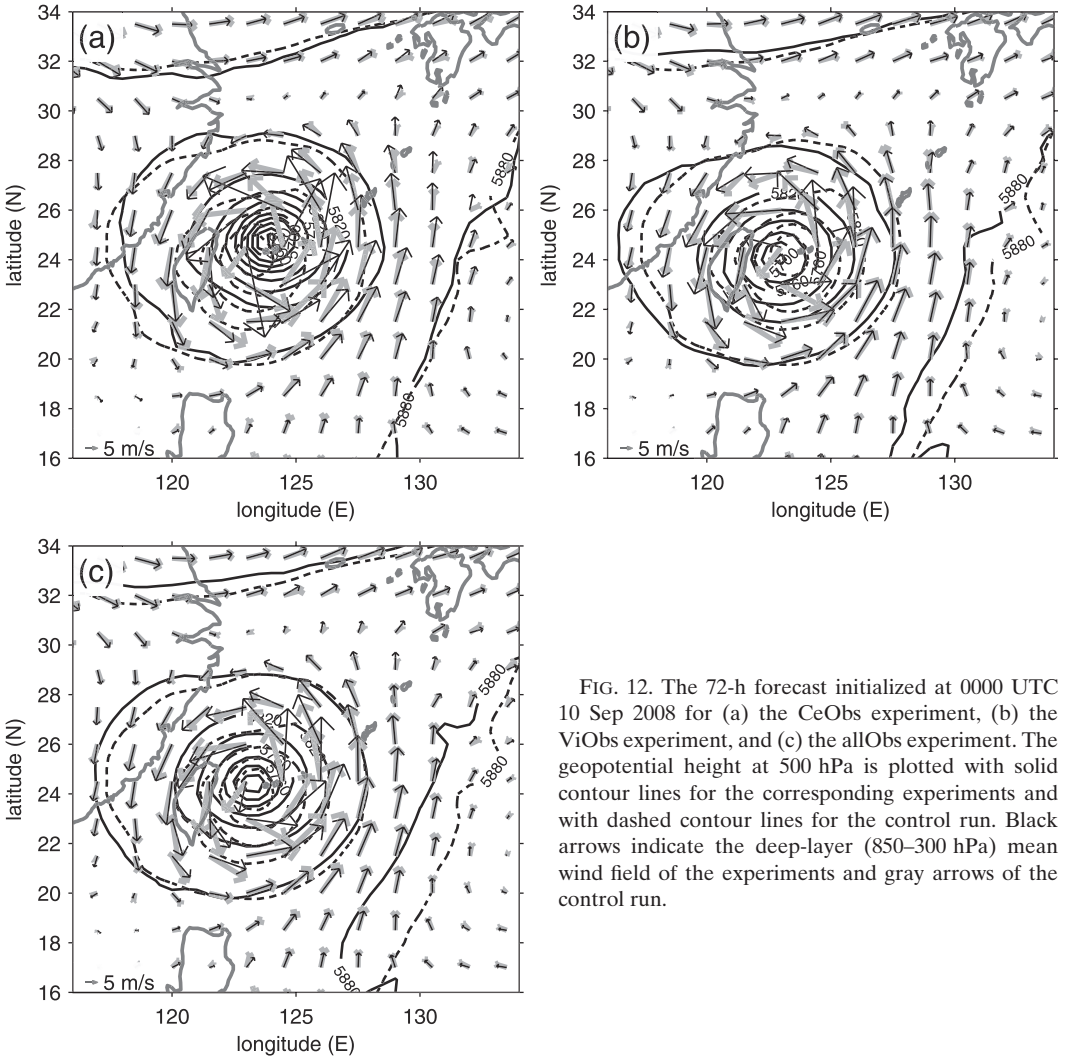

FIG. 12. The 72-h forecast initialized at 0000 UTC 10 Sep 2008 for (a) the CeObs experiment, (b) the ViObs experiment, and (c) the allObs experiment. The geopotential height at 500 hPa is plotted with solid contour lines for the corresponding experiments and with dashed contour lines for the control run. Black arrows indicate the deep-layer (850–300 hPa) mean wind field of the experiments and gray arrows of the control run.

global models with a resolution of 25 km or less cannot fully resolve the strong pressure gradient of a TC.

Figure 15 shows two examples of central MSLP forecasts. According to best-track data, Sinlaku reaches its minimum pressure of 935 hPa between 1200 UTC 10 September and 1200 UTC 11 September. All central MSLP forecasts show large errors up to 40 hPa during the most intense period. At 0000 UTC 10 September (Fig. 15a), the CeObs experiment decreases the central pressure and the pressure error is reduced more than 10 hPa compared to the control run. When Sinlaku is closer to land and begins to weaken at 84 and 60 h, respectively, it is obvious that the correct track forecast has an essential influence on the central pressure. Even though the CeObs experiment reduces the central MSLP error in the short range, the TC does not weaken from 3 days onward because of the wrongly predicted track. In contrast, the improved track forecast of ViObs is partly capable of decaying the system because the ViObs experiment predicts Sinlaku closer to its real position near Taiwan (cf. Fig. 7b). The experiments starting at 0000 UTC 11 September (Fig. 15b) only have a limited influence on central MSLP values during the most intense period of Sinlaku. Observations in the vicinity of the typhoon (ViObs) lead to the largest reduction of the central MSLP error. When the system begins to weaken after 60 h, larger improvements of the experiments are visible. These improvements, however, do not arise from a better intensity forecast in the short range, but rather from a better track forecast as for this case all experiments produce a track error reduction (see also Fig. 7c).

4. Discussion and summary

Data denial experiments were conducted with the ECMWF global model to assess the influence of targeted

TABLE 3. Track forecast errors (km) of all cases for Typhoon Sinlaku (2008). Boldface numbers indicate cases where a reduction of the mean 12–120-h track forecast error compared to the NoObs control run is achieved.

Date	Expt	12 h	24 h	36 h	48 h	60 h	72 h	84 h	96 h	108 h	120 h	Mean
0000 UTC	CeObs	16	29	29	19	73	59	120	232	353	573	**150**
9 Sep	NoObs	10	26	19	21	68	65	181	312	504	778	198
0000 UTC	ViObs	57	24	26	61	13	18	51	134	202	219	**80**
10 Sep	CeObs	18	59	47	54	80	141	197	284	467	545	189
	AllObs	3	55	46	72	24	64	155	225	370	448	146
	NoObs	45	9	7	52	28	34	141	197	338	400	125
0000 UTC	ReObs	13	44	51	18	91	161	208	257	382	585	**181**
11 Sep	ViObs	4	47	26	25	73	65	150	179	227	269	**106**
	AllObs	10	51	44	19	70	163	195	267	291	430	**154**
	NoObs	10	23	22	27	102	155	246	353	500	722	216
1200 UTC	ReObs	23	55	19	87	176	214	296	439	634	891	**283**
11 Sep	CeObs	14	40	35	89	146	216	306	474	760	1074	**315**
	AllObs	17	43	48	111	160	282	353	423	637	858	**293**
	NoObs	18	62	45	123	201	284	380	488	693	952	325
1200 UTC	CeObs	34	42	98	147	202	292	486	709	928	1041	**398**
12 Sep	NoObs	54	30	117	163	250	341	487	747	967	1084	424
0000 UTC	ReObs	18	51	57	78	99	73	84	144	227	315	115
14 Sep	NoObs	24	44	54	73	127	111	55	105	117	172	88
0000 UTC	ReObs	48	47	55	34	217	358	422	592	566	—	260
16 Sep	ViObs	41	47	50	68	209	336	436	623	571	—	265
	AllObs	33	43	49	71	232	372	508	611	570	—	277
	NoObs	43	63	48	48	196	316	413	611	525	—	252

dropsonde observations on typhoon track forecasts during T-PARC. The observations were separated into three subsets to investigate the influence of observations from different locations relative to the TC.

Observations in the vicinity of the TC (ViObs) lead to the largest track error reduction. Observations of this subset were mainly collected by the Taiwanese Astra Jet operated under the DOTSTAR research program. Previous studies with different models and different typhoon systems also showed a positive influence of these observations (Wu et al. 2005; Yamaguchi et al. 2009). One very important part of the flight strategy in the DOTSTAR program is to circumnavigate the storm during every flight mission, besides often sampling parts of sensitive regions. The ViObs subset for all cases, except at 0000 UTC 16 September, consists of observations that are located in a complete circle around the outer domain of the storm. Findings from Peng and Reynolds

TABLE 4. Track forecast errors (km) of all cases for Typhoon Jangmi (2008). Italic numbers indicate that the storm was located directly over Taiwan at this time and the storm position was estimated by the minimum of the geopotential height at 700 hPa instead of the minimum MSLP. Boldface numbers indicate cases where a reduction of the mean 12–120-h track forecast error compared to the NoObs control run is achieved.

Date	Expt	12 h	24 h	36 h	48 h	60 h	72 h	84 h	96 h	108 h	120 h	Mean
0000 UTC	CeObs	15	72	55	43	99	219	237	203	419	823	**219**
25 Sep	NoObs	36	24	30	36	104	201	217	326	502	935	241
0000 UTC	CeObs	7	83	145	248	224	283	306	—	—	—	**185**
26 Sep	NoObs	15	64	141	230	114	344	391	—	—	—	186
0000 UTC	ReObs	17	39	*45*	113	118	261	393	—	—	—	141
27 Sep	ViObs	7	19	*54*	81	83	232	293	—	—	—	**110**
	CeObs	11	18	*62*	79	153	369	482	—	—	—	168
	AllObs	13	37	*28*	35	118	314	367	—	—	—	**130**
	NoObs	18	27	*10*	109	159	299	322	—	—	—	135
0000 UTC	ReObs	*11*	10	44	118	150	—	—	—	—	—	67
28 Sep	ViObs	*30*	97	66	173	211	—	—	—	—	—	116
	AllObs	*40*	66	112	159	226	—	—	—	—	—	121
	NoObs	*28*	48	26	69	144	—	—	—	—	—	63
1200 UTC	ReObs	53	41	95	170	—	—	—	—	—	—	**90**
28 Sep	NoObs	52	37	141	247	—	—	—	—	—	—	119

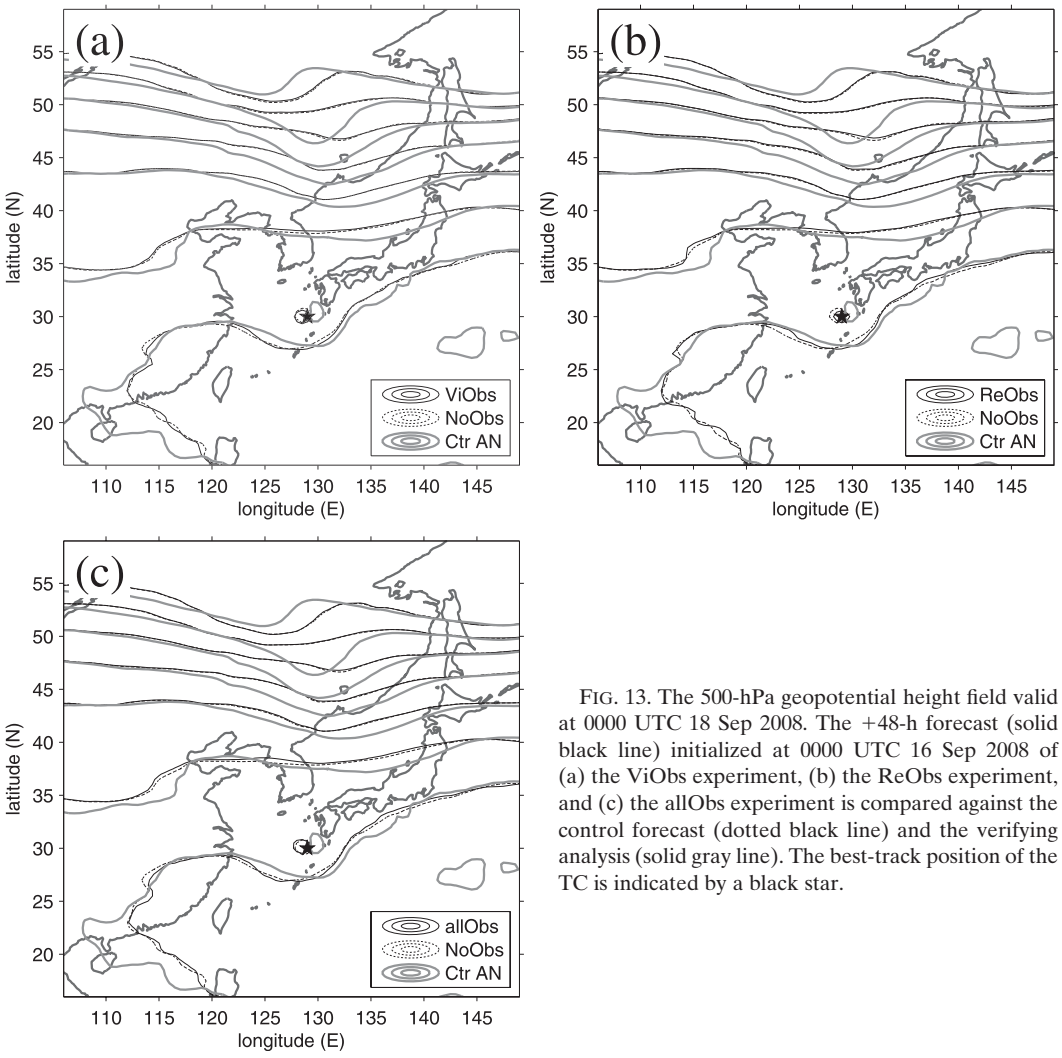

FIG. 13. The 500-hPa geopotential height field valid at 0000 UTC 18 Sep 2008. The +48-h forecast (solid black line) initialized at 0000 UTC 16 Sep 2008 of (a) the ViObs experiment, (b) the ReObs experiment, and (c) the allObs experiment is compared against the control forecast (dotted black line) and the verifying analysis (solid gray line). The best-track position of the TC is indicated by a black star.

(2006) and Reynolds et al. (2009) that track forecasts of TCs are sensitive to changes in the initial conditions at an annulus around the storm center at approximately 500 km are consistent with the positive influence of the ViObs observations.

Even if a large fraction of the remote dropsondes (ReObs) is located in areas indicated to be of increased sensitivity by SV computations, results from this experiment do not show a large improvement of the track forecast. Observations in remote sensitive regions mainly influence the analysis fields close to the subtropical anticyclone or in the midlatitudes, whereas the structure of the TC itself is only marginally affected. Changes to the remote environment of the TC do not have a large influence on the track forecasts of Sinlaku and Jangmi. The low influence could be related to small analysis errors and a comparably good representation of the large-scale flow around the TC in the ECMWF model due to the extensive use of satellite observations. Furthermore, the low resolution of the SV computations (T_L95 at ECMWF during T-PARC) might not correctly reflect sensitivity patterns. There are indications that sensitivity maxima shift closer to the storm itself with an increased resolution of SV calculations (S. Lang 2009, personal communication). Finally, the suboptimal sampling of the remote sensitive regions, with only parts of high and moderate sensitive regions covered, could also be a reason for the small influence of these dropsondes (Aberson 2003).

The ECMWF data assimilation system seems to be capable of handling extreme observations in the TC center (CeObs). The quality control works reliably and a large fraction of the data are flagged and rejected to minimize unrepresentative structures in the model. However, in terms of track forecast errors the influence is neutral on average. There is a significant case-to-case

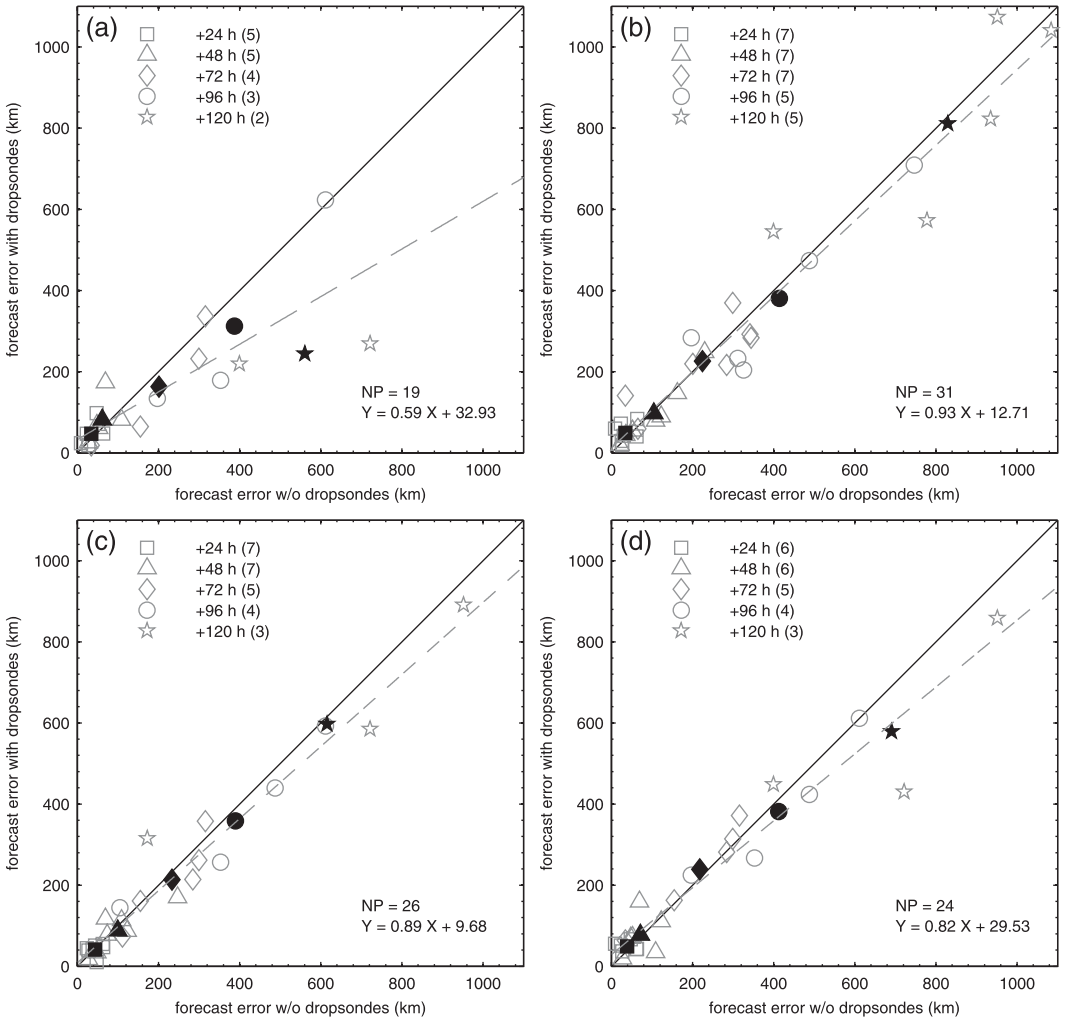

FIG. 14. Scatterplots of track forecast errors of experiments against the control run. The *x* axis shows the track errors of the NoObs control run, and the *y* axis shows the track errors of (a) ViObs, (b) CeObs, (c) ReObs, and (d) allObs experiments. The solid black line represents the 45° line with values below indicating an error reduction and values above an error increase compared to the control run. Different markers indicate different forecast times. Black solid markers represent mean values for the respective forecast step. The slope, the zero offset, and the used number of points (NP) of the linear regression line (gray dashed line) are displayed in the lower right.

variability with these observations and large positive (e.g., 0000 UTC 9 September) as well as negative (e.g., 0000 UTC 10 September) cases can be identified. Despite the information potentially provided by these data, future data assimilation systems have to solve several issues to fully exploit these observations. Unrealistic structures in the model analysis are sometimes introduced by the position offset of dropsondes. Up to now, dropsonde data are assimilated with one fixed position, but there can be a significant shift from the launch position during the descent in particular when they are placed in the eyewall region (Aberson 2008). Additionally, incomplete sampling of the TC center with dropsondes can introduce unrealistic asymmetries in the model resulting in wrong track forecasts. Track forecast degradations with dropsonde data from the center region have been found with the National Centers for Environmental Prediction (NCEP) Global Forecasting System (GFS) and no dropsonde data within a radius of 111.1 km (or 3 times the specified radius of maximum wind, whichever is larger) are used in the data assimilation system of the GFS as a consequence (Aberson 2008). An average positive influence with the allObs experiment is obtained, but not obligatory. The most beneficial results are achieved when combining all available observations.

Large differences in the results of the experiments in the pre- and postrecurvature period of a recurving TC are detected. During the prerecurvature period, a larger

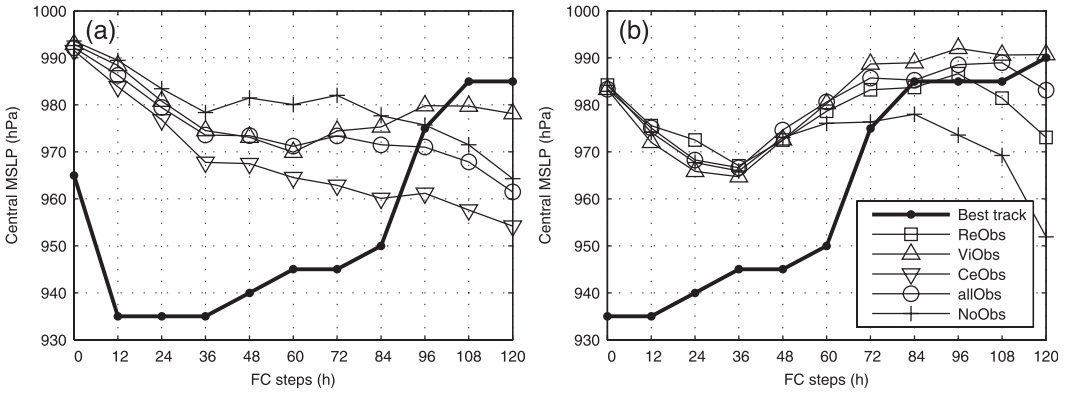

FIG. 15. Best-track data and central MSLP values of the experiment and control forecasts initialized at (a) 0000 UTC 10 Sep 2008 and (b) 0000 UTC 11 Sep 2008.

influence of the observations can be identified independent of the dropsonde subsets. Model errors in the structure change of the TC during landfall are expected, but improving the analysis of the typhoon and better forecasting the landfall point can minimize errors due to land interaction (Wu 2001). The influence of dropsondes for typhoon targeting was limited after recurvature and the representation of the upstream midlatitude flow field becomes more important for the propagation of the TC. Reynolds et al. (2009) showed that in cases of recurving TCs, sensitivity can be found to the northwest of the TC and sometimes can be located as far as 4000 km upstream over the Asian continent. For these cases, a modification of the initial conditions next and in the environment of the TC through dropsondes can only have a limited influence on the track forecast. Results may be different for other observational data types; for example, the Doppler wind lidar (Weissmann et al. 2005), which was operated on board the DLR Falcon during T-PARC. Weissmann and Cardinali (2007) demonstrated the value of this new type of observations for ECMWF forecasts in the midlatitudes.

Acknowledgments. The dropsonde data were collected as part of T-PARC, TCS08, and DOTSTAR. T-PARC and TCS08 were sponsored by an international consortium from the United States (National Science Foundation, Office of Naval Research, NRL, Air Force), Germany (DLR, Forschungszentrum Karlsruhe), Japan (Japanese Meteorological Agency), Korea (National Institute of Meteorological Research), and Canada (Environment Canada). The role of the National Center for Atmospheric Research (NCAR) Earth Observing Laboratory (EOL) for campaign and data management is acknowledged. DOTSTAR is funded by the National Science Council of Taiwan, the U.S. Office of Naval Research, and the Central Weather Bureau Taiwan. The authors are thankful to the aircraft dropsonde operators and all the people who contributed to the successful realization of T-PARC, TCS08, and DOTSTAR. In particular, we acknowledge the tireless efforts of the crews of the 53rd Weather Reconnaissance Squadron/Air Force Reserve Command, the NRL Scientific Development Squadron ONE (VXS-1), and the DOTSTAR and the DLR Falcon aircraft. The support of various people at ECMWF for the experiments and ECMWF computing resources and the ECMWF efforts in providing the Data Targeting System software and Web site are greatly appreciated. In particular, the authors acknowledge the help of Carla Cardinali and the reprocessing of the dropsonde data by Milan Dragosavac and Ioannis Mallas. This work is part of the Deutsche Forschungsgemeinschaft (German Research Foundation) research unit Predictability and Dynamics of Weather Systems in the Atlantic–European Sector (PANDOWAE; more information is available online at http://www.pandowae.de). The authors are thankful to George Craig (DLR) and Oliver Reitebuch (DLR) for helpful comments on the manuscript.

REFERENCES

Aberson, S. D., 2002: Two years of operational hurricane synoptic surveillance. *Wea. Forecasting,* **17,** 1101–1110.

——, 2003: Targeted observations to improve operational tropical cyclone track forecast guidance. *Mon. Wea. Rev.,* **131,** 1613–1628.

——, 2008: Large forecast degradations due to synoptic surveillance during the 2004 and 2005 hurricane seasons. *Mon. Wea. Rev.,* **136,** 3138–3150.

Andersson, E., and H. Järvinen, 1999: Variational quality control. *Quart. J. Roy. Meteor. Soc.,* **125,** 697–722.

Buizza, R., and A. Montani, 1999: Targeting observations using singular vectors. *J. Atmos. Sci.,* **56,** 2965–2985.

Burpee, R. W., J. L. Franklin, S. J. Lord, R. E. Tuleya, and S. D. Aberson, 1996: The impact of omega dropwindsondes

on operational hurricane track forecast models. *Bull. Amer. Meteor. Soc.,* **77,** 925–933.

Elsberry, R. L., and P. A. Harr, 2008: Tropical Cyclone Structure (TCS08) field experiment science basis, observational platforms, and strategy. *Asia-Pacific J. Atmos. Sci.,* **44,** 209–231.

Järvinen, H., and P. Undèn, 1997: Observation screening and background quality control in the ECMWF 3DVar data assimilation system. ECMWF Tech. Memo. 236, 34 pp.

Klinker, E., F. Rabier, G. Kelly, and J.-F. Mahfouf, 2000: The ECMWF operational implementation of four-dimensional variational assimilation. III: Experimental results and diagnostics with operational configuration. *Quart. J. Roy. Meteor. Soc.,* **126,** 1191–1215.

Langland, R. H., 2005: Issues in targeted observing. *Quart. J. Roy. Meteor. Soc.,* **131,** 3409–3425.

Mahfouf, J.-F., and F. Rabier, 2000: The ECMWF operational implementation of four-dimensional variational assimilation. II: Experimental results with improved physics. *Quart. J. Roy. Meteor. Soc.,* **126,** 1171–1190.

Majumdar, S. J., S. D. Aberson, C. H. Bishop, R. Buizza, M. S. Peng, and C. A. Reynolds, 2006: A comparison of adaptive observing guidance for Atlantic tropical cyclones. *Mon. Wea. Rev.,* **134,** 2354–2372.

Parsons, D., P. Harr, T. Nakazawa, S. Jones, and M. Weissmann, 2008: An overview of the THORPEX-Pacific Asian Regional Campaign (T-PARC) during August–September 2008. Preprints, *28th Conf. on Hurricanes and Tropical Meteorology,* Orlando, FL, Amer. Meteor. Soc., 7C.7.

Peng, M. S., and C. A. Reynolds, 2006: Sensitivity of tropical cyclone forecasts as revealed by singular vectors. *J. Atmos. Sci.,* **63,** 2508–2528.

Rabier, F., H. Jarvinen, E. Klinker, J.-F. Mahfouf, and A. Simmons, 2000: The ECMWF operational implementation of four-dimensional variational assimilation. I: Experimental results with simplified physics. *Quart. J. Roy. Meteor. Soc.,* **126,** 1143–1170.

Reynolds, C. A., M. S. Peng, S. J. Majumdar, S. D. Aberson, C. H. Bishop, and R. Buizza, 2007: Interpretation of adaptive observing guidance for Atlantic tropical cyclones. *Mon. Wea. Rev.,* **135,** 4006–4029.

——, ——, and J.-H. Chen, 2009: Recurving tropical cyclones: Singular vector sensitivity and downstream impacts. *Mon. Wea. Rev.,* **137,** 1320–1337.

Van der Grijn, G., J. E. Paulsen, F. Lalaurette, and M. Leutbecher, 2005: Early medium-range forecasts of tropical cyclones. *ECMWF Newsletter,* No. 102, ECMWF, Reading, United Kingdom, 7–14.

Weissmann, M., and C. Cardinali, 2007: Impact of airborne Doppler lidar observations on ECMWF forecasts. *Quart. J. Roy. Meteor. Soc.,* **133,** 107–116.

——, R. Busen, A. Dörnbrack, S. Rahm, and O. Reitebuch, 2005: Targeted observations with an airborne wind lidar. *J. Atmos. Oceanic Technol.,* **22,** 1706–1719.

Wu, C.-C., 2001: Numerical simulation of Typhoon Gladys (1994) and its interaction with Taiwan terrain using the GFDL hurricane model. *Mon. Wea. Rev.,* **129,** 1533–1549.

——, and Coauthors, 2005: Dropsonde observations for typhoon surveillance near the Taiwan region (DOTSTAR): An overview. *Bull. Amer. Meteor. Soc.,* **86,** 787–790.

——, J.-H. Chen, P.-H. Lin, and K.-H. Chou, 2007a: Targeted observations of tropical cyclone movement based on the adjoint-derived sensitivity steering vector. *J. Atmos. Sci.,* **64,** 2611–2626.

——, K.-H. Chou, P.-H. Lin, S. D. Aberson, M. S. Peng, and T. Nakazawa, 2007b: The impact of dropwindsonde data on typhoon track forecasts in DOTSTAR. *Wea. Forecasting,* **22,** 1157–1176.

——, and Coauthors, 2009: Intercomparison of targeted observation guidance for tropical cyclones in the northwestern Pacific. *Mon. Wea. Rev.,* **137,** 2471–2492.

Yamaguchi, M., T. Iriguchi, T. Nakazawa, and C.-C. Wu, 2009: An observing system experiment for Typhoon Conson (2004) using a singular vector method and DOTSTAR data. *Mon. Wea. Rev.,* **137,** 2801–2816.